Errors in shearography measurements due to the creep of the PZT shearing actuator

Filip Zastavnik[1,*], Lincy Pyl[1], Jun Gu[1], Hugo Sol[1], Mathias Kersemans[2], Wim Van Paepegem[2]

[1] Department Mechanics of materials and construction, Vrije Universiteit Brussel, Pleinlaan 2, 1050 Brussels, Belgium

[2] Department of Materials science and engineering, Universiteit Gent, Technologiepark-Zwijnaarde 903, 9052 Zwijnaarde, Belgium

[*] Corresponding author: filip.zastavnik@vub.ac.be

Abstract

Shearography is a modern optical interferometric measurement technique. It uses interferometric properties of coherent laser light to measure deformation gradients on the μm/m level. In the most common shearography setups, the ones employing Michelson interferometer, the deformation gradients in both x- and y-direction can be identified by setting angles on the shearing mirror. One of the mechanisms for setting the desired shearing angles in the Michelson interferometer is using the PZT actuators. This paper will reveal that the time-dependent creep behaviour of the PZT actuators is a major source of measurement errors. Measurements at long time spans suffer severely from this creep behaviour. Even for short time spans, which are typical for shearographic experiments, the creep behaviour of the PZT shear actuator induces considerable deviation in the measured response. In this paper the mechanism and the effect of the PZT creep is explored and demonstrated with measurements. For long time-span measurements in shearography, noise is a limiting factor. Thus, the time-dependent evolution of noise is considered in this paper, with particular interest in the influence of the external vibrations. Measurements with and without the external vibration isolation are conducted and the difference between the two setups is analyzed. At the end of the paper some recommendations are given for minimizing and correcting the here studied time-dependent effects.

1 Introduction

Shearography [1, 2] is an interferometric full-field measurement technique that yields the gradient of deformation of the inspected surface. The main advantage of shearography, as compared to similar measurement techniques as Electronic Speckle Pattern Interferometry (ESPI) [3], is its relative insensitivity to external vibrations. Indeed, the measurement of the displacement gradient does not suffer from rigid body displacements. This enables shearography to be used qualitatively in industrial environments. From its conception [4, 5] shearography was envisioned as a quantitative technique to determine strains, but presently it is mostly used as a

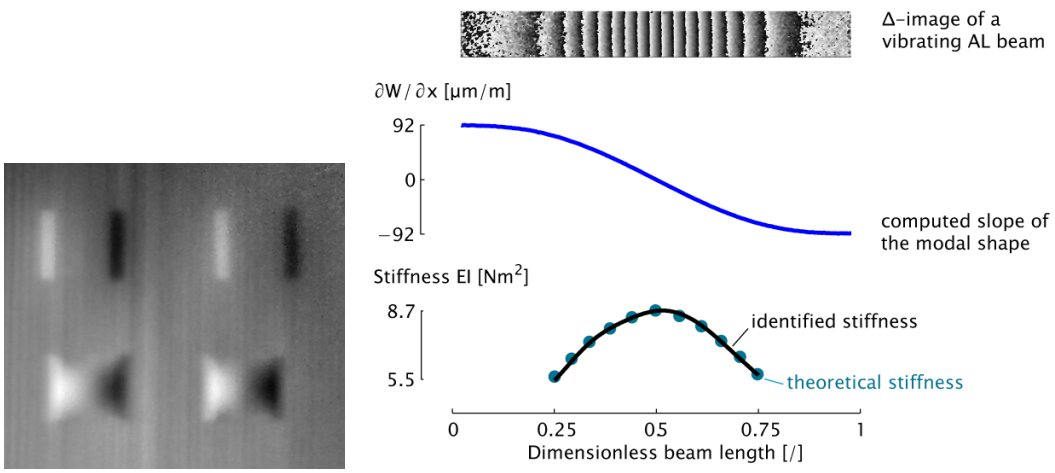

Figure 1: Examples of qualitative (a) and quantitative shearography (b). Four intentional subsurface delaminations in a composite plate are revealed by thermally loading the surface and visualizing it with shearography (a). The local bending stiffness of a vibrating aluminium beam with variable thickness is calculated from a shearography image [15] (b).

qualitative technique, to visualize defects in materials [6]. It is used, among others, as a non-destructive testing (NDT) technique, in health monitoring of aircraft structures [7, 8], for inspection of bonding quality in joints [9] and reinforcement of concrete beams [10]. Shearography has become widely used for defect detection in the pneumatic tire industry [11]. Visual inspection can be enhanced numerically by determining the size and depth of a defect [12]. The qualitative use relies on the operator skill to assess the resulting shearography images and to visually detect defects. Figure 1a shows an example of detection of delamination in a composite plate.

Fewer quantitative applications exist, and are mostly focused on quantitive strain measurement [13] and object slope measurements [14]. An example of quantitative application of shearography is also the identification of local stiffness values in beam specimens shown in figure 1b [15].

Similar to other interferometric technologies, shearography is subject to high levels of noise. Noise is detrimental for both qualitative (as features become hard to distinguish visually) and quantitative measurements (as the measured values can be drowned in the noise). Unwrapping algorithms [16], necessary for quantitative shearography, usually tolerate only a small amount of noise. Relatively high resolution of shearography enables the use of de-noising (filtering) methods [2, 17], but their effectiveness is not without limits. Most of the noise in shearography is due to the speckle decorrelation [18], an effect that occurs when the interference pattern ("speckles") shifts related to the shearography camera during measurement. The speckle decorrelation can occur due to high deformation of the observed object, relative change in the distance between the laser source, camera

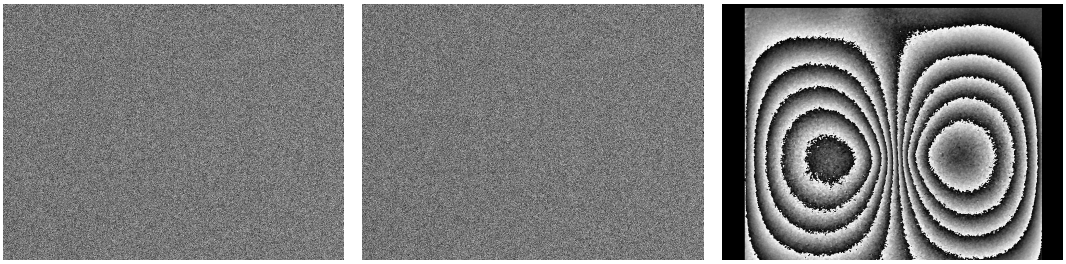

(a) Φ_1 (b) Φ_2 (c) $\Delta = \Phi_2 - \Phi_1$

Figure 2: An example of a generic shearography measurement – a flat plate loaded by a local force in the center. The Φ-images before (a) and after deformation (b) are used to produce a Δ-image (c), corresponding to the out-of-plane gradient $\partial w/\partial x$

and the object, and because of the change of the refractive index of the medium between them.

Error sources in shearography are the local (i.e. dependent on the location in the shearography image) sensitivity variation and the local shearing distance variation. In shearography, the sensitivity to the displacement gradients is influenced by the positioning of the light source and the shearography camera, relative to the specimen. Thus for a specimen of a finite size, the sensitivity will vary locally. The shearing distance (as shown later) is one of the most important variables in quantifying the results of shearography measurements. The shearing distance can vary across the captured image if the measured surface is not planar, or because of optical distortions in the shearography camera. For quantitative measurements, effects of these local variations need to be checked and, if possible, corrected for [19, 20].

Each shearography measurement consist of making two so-called Φ-images, before and after the loading, as shown in figure 2a and 2b). The Φ-images contain the wrapped phase maps, which in term are generated from a series of phase-shifted images of the speckle pattern. Subtraction of the two Φ-images produces the Δ-image. A Δ-image contains a wrapped image of the displacement gradients (see figure 2c). The specifics of the Φ- and the Δ-images are discussed in more detail in the following section. The time interval for producing the two Φ-images is fixed for a given equipment and measuring conditions, but the time it takes to deform the specimen is variable (case dependent). When deformation is due to thermal loading [21], the time interval can be considerably lengthened. Because of the sensitivity of shearography, the external effects, the environmental vibrations and the air flow between the camera and the specimen can cause an increase of noise. This increase of noise worsens as the measurements become longer. In this paper, the progressively increasing noise and the influence of isolating the environmental vibrations are demonstrated and quantified. Commonly, it is claimed that shearography can be used in industrial applications, as the external influences are minimal. However, the results presented in this paper demonstrate that the time interval for the measurements needs to be very short, or the external

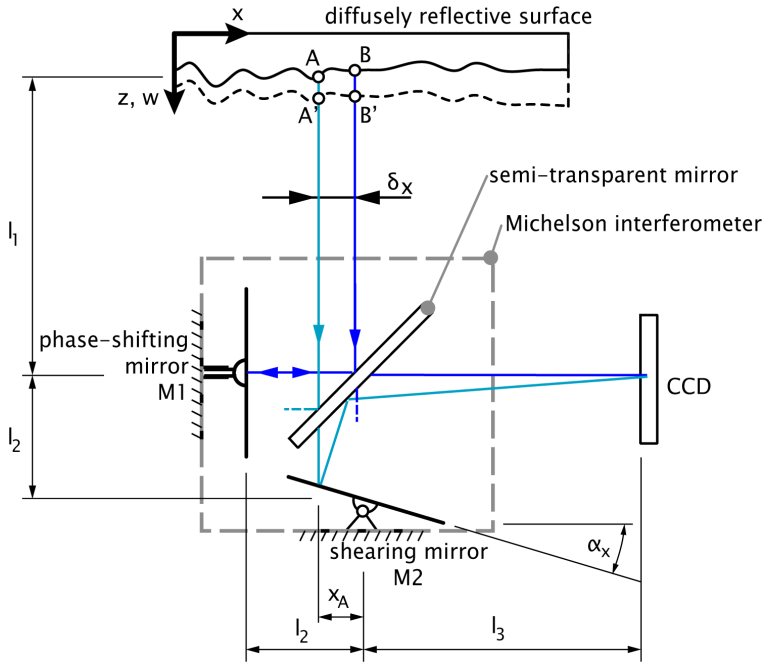

Figure 3: Working principle of shearography using the Michelson interferometer – points A and B are superimposed onto the imaging sensor (CCD)

influences must be sufficiently dampened, in order not to exceed the acceptable levels of noise.

Two mirrors used in the Michelson interferometer of the shearography camera are the rotating shearing mirror and the translating phase-shifting mirror (see figure 3). The shearing mirror in the Michelson interferometer can be rotated mechanically, by a screw, or by a piezoelectric element. In the commercial systems, it is often practical to move the control of the shearing away from the optical system and into the external control unit or even have the shearing control implemented in the software. Thus, a piezoelectric actuation of the shearing distance can be often found in commercial systems. The shearography setup used in this paper has the shearing actuated by a piezo-electric element, and is controlled in the software. The translation of the phase-shifting mirror is commonly actuated by a piezoelectric-element in all shearography systems with the Michelson interferometer. The reason for using piezoelectric materials is that the actuation distance of the two mirrors needs to be very small. In the setup used in this paper, the shearing mirror rotates in increments of 0.01 mrad, while the phase-shift mirror translations are on the level of 0.1 µm (fractions of the wavelength of laser light). The PZT, or lead zirconate titanate $Pb[Zr_xTi_{1-x}]O_3$, is one of the world's most widely used piezoelectric ceramic materials. The non-linearity, hysteresis and the linear drift of the response of the PZT are discussed in literature, and a variety of phase-shifting techniques is developed to compensate for the errors associated with the phase-shifting mirror [1, 22, 23, 24]. The phase-shifting techniques used for shearography are similar for ESPI [3].

The errors related to the shearing mirror in shearography, arising from the

non-linearity, hysteresis and the linear drift, are usually not considered to have a meaningful impact on the measurement as the mirror moves only once, before the measurement. However, the creep response of PZT, recently discussed in literature [25], could have a significant impact on the accuracy of the shearography measurements. The main mechanism inducing the creep behavior in PZT is a phenomenon called the domain switching. The domain switching are the changes in the polarization state in the PZT material, when a material grain in the PZT changes from one spontaneously polarized state to another under electrical or mechanical load. In [25], the creep was modeled using the power law, $S_c = \beta_1 t^n$, where the S_c is the creep strain and the t is the time. The two fitting parameters, β_1 and n, both depend on the magnitude of the external load.

In this paper the time-dependent effects, related to the duration of the shearography experiments, will be discussed. It is shown that the duration of the experiment can have a considerable impact on the measurement through the systematic error, produced by the creep of the PZT. Noise in the measurements, influenced by environmental vibration, also increases with time. Both of these time-dependent effects are discussed and quantified. An evident measure to minimize the influence of external vibrations is placing the whole measurement setup, including the loaded object onto a vibration isolating table. The influence of the external vibrations is quantified by comparing the noise in the images using the same setup, with and without the vibration isolation. A very simple quantification principle is developed, that can be universally applied before any shearography measurement, to estimate the uncertainty related to the creep of the PZT and the external vibrations.

In the rest of the first section, a general overview of the principle of shearography is given. The principle and the equations are presented in such a way as to simplify the demonstration of the effect of the PZT creep further in the paper. Next, the effect of the change of the shearing distance during the experiment will be demonstrated theoretically, and verified experimentally. Another time-dependent effect is the noise in the measurements. A method for quantifying the level of noise and its time-dependent evolution is developed and demonstrated by measurements. This method is then applied on a shearography setup, with and without the external vibration isolation, to quantify the difference in the noise. At the end of the paper, some recommendations are given as to how to minimize the influence of the PZT creep and the noise on the shearography measurements.

Principle of shearography

An out-of-plane measurement setup will be used to describe the principle of operation of shearography. The coordinate system used in this paper has the z-direction as the out-of-plane direction, with the x- and the y-coordinate being the in-plane directions. u, v and w are the displacements in the x-, y- and z-direction respectively. The shearography images all have the x-direction as the horizontal and the y-direction as the vertical axis. Shearography produces an image which is proportional to the $\partial w/\partial\{x, y\}$ – the gradients of the out-of-plane displacement of the observed surface. In-plane shearography configurations can additionally

produce images corresponding to the $\partial\{u, v\}/\partial\{x, y\}$ gradients but they are not discussed here. The shearography image, called the Δ-image, is calculated as a subtraction of two phase-images, the Φ-images. One Φ-image represents a map of phase shifts between pairs of sheared points. Usually, the first Φ-image represents the undeformed surface, and the second Φ-image the deformed surface. As such, $\Delta = \Phi_2 - \Phi_1$ is a representation of the deformation between the two Φ-images.

Figure 2 shows the steps for producing a shearography image. The phase difference in a Φ-images is in the range $(0, 2\pi)$, and can only be resolved within this range. If the phase difference goes outside this range, it will be "wrapped" back into it, i.e. a $\pm 2n\pi$ phase shift will be superposed (n being an integer number), so the phase difference is again within the range $(0, 2\pi)$. Similarly, the Δ-image is in the range $(-\pi, \pi)$, and values outside the range are wrapped into it. The effect of wrapping can be seen in the figure 2c. The fringes seen in the Δ-image are the sudden phase jumps between $-\pi$ and π. Unwrapping algorithms [16] have been developed that recognize these jumps and introduce $\pm 2n\pi$ corrections to recover the original, non-wrapped, values.

In the figure 3 the principle of shearography is illustrated. A shearing mirror, in the Michelson interferometer, is used to project two points from the observed surface to the electronic CCD image sensor of the camera. Light entering the Michelson interferometer is split by the semi-transparent mirror. Half of the light beam passes through it, while the other half is reflected. The light reflected from the semi-transparent mirror is reflected again by the phase-shifting mirror M1 onto the CCD imaging sensor. Phase-shifting is a technique used to reconstruct the phase of the light wave from the measurements by the CCD sensor in the shearography camera, but is outside the scope of the paper. For details see [1, 2]. The light that passed through the semi-transparent mirror is reflected by the shearing mirror M2, over the semi-transparent mirror, onto the CCD imaging sensor. Because the shearing mirror M2 is under a slight angle α_x, on the point (pixel) of the CCD sensor shown in the figure 3, light from A and B will be superimposed. The superimposition for points A and B depends on their mutual phase shift because coherent, laser light is used. The superimposition of light will create an interference pattern, registering as different intensities on the CCD sensor. From the intensity registered by the imaging sensor, the interference phase shift can be calculated. Points A and B are separated by the shearing distance δ_x, a distance which is proportional to the shearing angle α_x, as

$$\delta_x = 2(l_1 + 2l_2 + l_3)\alpha_x \tag{1}$$

where distance l_1 is the distance between the surface and the center of the interferometer, and l_2 and l_3 are the distances shown in figure 3.

For points A and B, the undeformed state of surface, the phase shift $\Phi(A, B) = \phi(A) - \phi(B)$, where ϕ is the absolute phase of the light wave. The absolute phases of A and B can not be measured by shearography, only the phase shift $\Phi(A, B)$ between them. After the phase map $\Phi(A, B)$ is measured, a surface is deformed or displaced, and a new phase shift $\Phi(A', B')$ is measured, where point A is displaced into A' and B into B'. The setup illustrated in figure 3 is sensitive to w, the displacement in the z-direction, which changes the z-coordinate of the points

as $z_{A'} = z_A + w_A$ and $z_{B'} = z_B + w_B$. The displacement in the z changes the light paths from the light source (not shown in figure 3, but same location as the camera) over A and B to the CCD by $2\,w_A$ and $2\,w_B$, which is equivalent to absolute phase changes of points A and B

$$\begin{aligned}\phi(A') &= \phi(A) + \frac{4\pi}{\lambda} w_A \\ \phi(B') &= \phi(B) + \frac{4\pi}{\lambda} w_B\end{aligned} \tag{2}$$

After deformation the phase shift becomes

$$\Phi(A',\, B') = \left[\phi(A) + \frac{4\pi}{\lambda} w_A\right] - \left[\phi(B) + \frac{4\pi}{\lambda} w_B\right] \tag{3}$$

Phases $\Phi(A,\, B)$ and $\Phi(A',\, B')$ by themselves are not revealing anything about the deformation, but their difference

$$\begin{aligned}\Delta &= \Phi(A',\, B') - \Phi(A,\, B) \\ &= \frac{4\pi}{\lambda}(w_B - w_A)\end{aligned} \tag{4}$$

is the relative phase displacement of the points A and B after the deformation. The phase difference multiplied by the wavelength of the light, $(\lambda/4\pi)\Delta$ is the relative displacement of point A compared to the point B. Divided by the distance between the points A and B, the shearing distance δ_x (and provided it is small), it is a discrete gradient of the surface displacement. Δ is computed for each point on the imaging sensor, so $\Delta(x,\, y)$ is called the Δ-image:

$$\frac{\partial}{\partial x} w(x, y) = \frac{\lambda}{4\pi\delta_x} \Delta(x, y) \tag{5}$$

The shearing mirror M2 can also rotate in the perpendicular, y-direction, and an angle α_y causes the shear distance δ_y. In that case the Δ-image is sensitive to the gradient of deformation $\partial w/\partial y$ and yields:

$$\frac{\partial}{\partial y} w(x, y) = \frac{\lambda}{4\pi\delta_y} \Delta(x, y) \tag{6}$$

Equations 5 and 6 are the simplified governing shearography equations, assuming camera and laser are co-linear and perpendicular to the measured surface. The principle explained here is simplified but will allow understanding of the main discussions in the paper. A more in-depth explanation of shearography can be found in [1, 2].

For the shearography image to be properly captured, the deformation (or the displacement) of the surface needs to be small. The speckle patterns, interference patterns created by laser lights reflected from the surface of the specimen, in the two Φ-images need to be correlated so that the subtraction $\Delta = \Phi_2 - \Phi_1$ yields

a meaningful result. In case of small deformations, there will be some decorrelation which produces noise in the images, which is normal. As the decorrelation becomes larger, the noise increases, until at one point the total decorrelation occurs. Subtracting two uncorrelated Φ-images results in pure noise, i.e. the result is meaningless. It is possible to control the size of the speckles, and when the speckles are larger, the measurement is less sensitive to decorrelation. However, to get the most information from the measurement, the speckles should be around the size of a camera pixel. In that case, an in-plane displacement of one pixel results in total decorrelation.

The next section will demonstrate the effect on the measurement of the change in the shearing distance due to the creep of the PZT shearing actuator.

2 Effect of change in the shearing distance during the measurement

Consider a shearing angle $\alpha_x = \alpha_{0x} + \alpha_{Cx}$, where α_{0x} is the initial intentional shearing angle and α_{Cx} is the time-dependent change in the angle, induced by the creep of the PZT actuator. For a single measurement, consisting of Φ_1 and Φ_2, the shearing angles will be $\alpha_x = \alpha_{0x}$ for Φ_1 and $\alpha_x = \alpha_{0x} + \alpha_{Cx}$ for Φ_2 at time $t = T$. If the creep-induced angle α_{Cx} between the Φ_1 and Φ_2 is large, a total decorrelation will occur and no Δ-image will be obtained. The value of the creep-induced angle to cause a total decorrelation, depends on the measurement setup. In general, the shearing angle change that displaces measurement Φ_2 by 1 pixel compared to the Φ_1 will cause a total decorrelation.

A rotation of the shearing mirror influences not only the shearing distance δ_x, but also shortens the path of a light beam from point A. When this shortening of the path occurs between capturing the Φ_1 and the Φ_2, it is analogous to displacing the point A, relatively to the point B. It can be seen in figure 3 that, as the shearing mirror M2 changes the angle for the α_{Cx} between the two Φ-images, it shortens the path of the light from point A by $2\alpha_{Cx}\, x_A$. x_A is the distance from the hinge of the shearing mirror M2 to the point where light from A reflects from the mirror M2, as illustrated in figure 3. The shortening of the light path can be considered as the phase change of the light wave from point A by $(4\pi/\lambda)\,\alpha_{Cx}\, x_A$.

At time $t = 0$ the phase difference will be

$$\Phi(0) = \phi(A) - \phi(B) \tag{7}$$

while at time $t = T$ (provided there was no actual displacement of the points A and B) it will be

$$\Phi(T) = \left[\phi(A) - \frac{4\pi}{\lambda}\alpha_{Cx}\, x_A\right] - \phi(B) \tag{8}$$

Their difference will register as a parasitic signal (systematic error)

$$\begin{aligned}\Delta_C &= \Phi(T) - \Phi(0) \\ &= -\frac{4\pi}{\lambda}\alpha_{Cx}\, x_A \\ &= -\frac{4\pi}{\lambda}\alpha_{Cx}\,(x - x_H)\end{aligned} \tag{9}$$

where the x_H is the x-coordinate of the hinge supporting the shearing angle, such that $x_A = x - x_H$.

The creep of the angle that controls the shearing distance in the y-direction will have analogous effects, so when they are both taken into account, the parasitic signal is

$$\Delta_C(x, y) = -\frac{4\pi}{\lambda}\left[\alpha_{Cx}\,(x - x_H) + \alpha_{Cy}\,(y - y_H)\right] \tag{10}$$

The previous equation reveals that the parasitic signal induced by creep of the PZT-controlled shearing mirror creates a bi-linear field across the image, with a zero at the position of the hinge of the shearing mirror, at $\{x_H, y_H\}$.

In case there is both deformation and a time-dependent change of the angles of the shearing mirror, linearity prescribes that the difference $\Phi(A',\, B',\, T) - \Phi(A, B, 0)$ equals $\Delta_{\text{correct}} + \Delta_C$. This means that, if the parasitic signal Δ_C caused by the creep of the PZT is known or measured, it can be simply subtracted from the obtained Δ-image.

The exact influence of the PZT creep depends on the placement of the mirrors and the CCD sensor in the shearography camera, and the distance to the measured surface. In this paper, an aluminium plate is studied in a certain time frame, without deforming it between the Φ_1 and Φ_2 images. The shearography setup used for these measurements, has the imaged surface resolution of 0.134 mm/pixel at the distance $l_1 + 2l_2 + l_3 = 1200$ mm. The shearing distance taken is $\delta_x = 3.39$ mm, which corresponding to the mirror angle of $\alpha_x = 1.45$ mrad. A creep angle of $\alpha_{xC} = 0.058$ mrad would then cause total decorrelation (4% change of the α_x during measurement), as the point A would be displaced by a pixel and the interference pattern would change completely and, for all intents and purposes, randomly. For this setup, a mirror angle change α_{Cx} that would produce a parasitic signal over the image from $-\pi$ to π is $\alpha_x = 0.008$ mrad (0.6% change of the α_x during measurement).

In the following section, the effect of the PZT shearing creep, described by the equation 10, is demonstrated experimentally. In addition, the time-dependent progression of the creep, after a change in the shearing distance, is investigated and discussed.

3 Measurements and evaluation of the creep of the shearing actuator

To quantify the creep of the PZT actuator, Δ-images of a flat aluminium plate are created, but without imposing any deformation or displacement on the measured

surface. Logically, the Δ-images should be a flat zero-valued image. However, it is shown that a time-dependent parasitic signal is measured, related to the creep of the PZT actuators controlling the shearing distance.

The shearography measurement system can be placed on an active vibration-isolating table. The table is pneumatically actuated and limits the environmental vibrations during measurements. To minimize the vibration and air-current based disturbance while doing measurement, no movement of persons is allowed in the lab. The importance of vibration isolating during measurements is highlighted in section 4, where the difference in measurements with and without the vibration isolation is quantified. The shearography instrument is in room with a stable temperature condition and the devices were allowed to come to working temperature before the measurements started.

The shearography setup used is an *isi-sys SE3 system*, with its software package *isi-sys studio*. The whole field-of-view of the camera is within the surface of the aluminium plate - the plate's area is 300×300 mm^2 and the imaged area of interest is 186×139 mm^2, corresponding to 1392×1040 pixels. The image is focused and parameters – aperture, sensor gain, exposure time – set to provide a clear image. The laser light used has a wavelength of $\lambda = 658$ nm (red color).

Figure 4a shows that the Δ-image with no deformation between Φ_1 and Φ_2 images contains a PZT creep parasitic signal. Visually, the image has a clear trend, as values seem to decrease from left to right over the x-direction, with little to no change in the y-direction. The effect of the PZT creep over the x-direction is dominant as the shearing is set in the x-direction. The two trends, for the x- and the y-direction, are computed using the medians m_x and m_y over the y- and x-direction respectively:

$$\begin{aligned} m_x(x,\, \Delta) &= \text{med}\,[\Delta(x = \text{const}, y)] \\ m_y(y,\, \Delta) &= \text{med}\,[\Delta(x, y = \text{const})] \end{aligned} \tag{11}$$

The medians m_x and m_y in figure 4a show a linear trend, which is consistent with equation 10. The error induced by the PZT creep can be fitted in the least-square sense by a bilinear function, such that

$$\Delta_{C\text{fit}}(x, y) = C_x\,(x - x_H) + C_y\,(y - y_H) \tag{12}$$

where the C_x and C_y are the fitting factors and the x_H and y_H are the locations of the hinge, a point around which the shearing mirror performs the rotation. In equation 12 the terms C_x and C_y are equivalent to $-(4\pi/\lambda)\,\alpha_C x$ and $-(4\pi/\lambda)\,\alpha_C y$ from equation 10. Influence of the creep can be corrected for by subtracting the fitted error $\Delta_{C\text{fit}}$ from the measured delta image

$$\Delta_{\text{correct}} = \Delta - \Delta_{C\text{fit}} \tag{13}$$

after which the Δ_{correct} should contain nothing but noise, as there was no actual deformation or displacement of the observed surface. This is demonstrated in figure 4b.

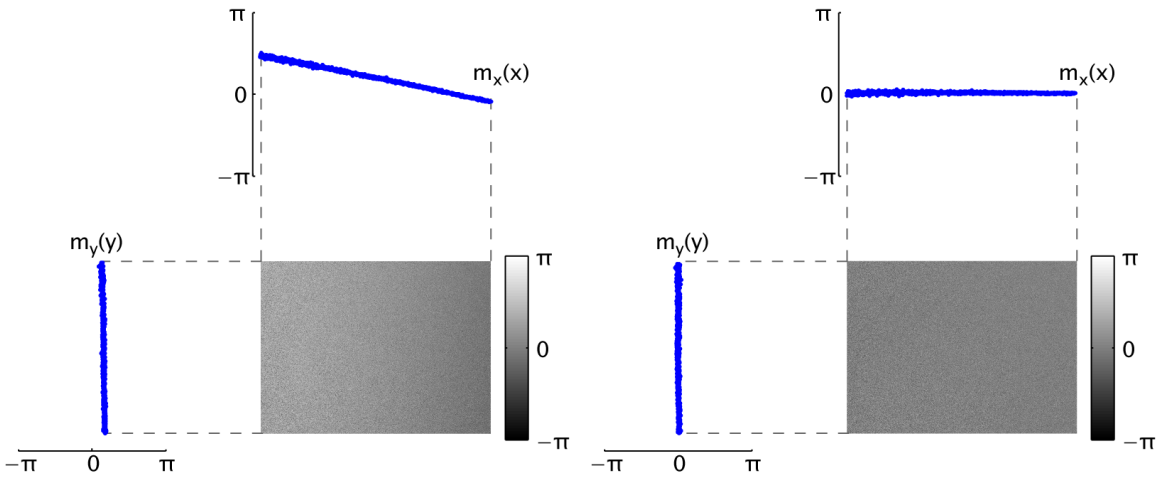

(a) Δ (b) Δ_{CORRECT}

Figure 4: A Δ-image with no deformation between the Φ_1 and the Φ_2 images, shows the parasitic signal induced by the PZT creep (a). Above and to the left of the image are plots of medians m_x and m_y. After removing the influence of the creep, the Δ_{CORRECT} (b) shows no trend in the medians m_x and m_y.

To test the effect of creep of the PZT shear actuator, parasitic gradients after changing the shear in the x-direction were measured. Again, no deformation nor displacement is imposed on the measured surface, so only parasitic signal Δ_C is present. Before the test, the shearing distance was kept at $\delta_x = 0$ for 600 s. The shearing distance was set to $\delta_x = 5.1$ mm (= 30% of max shear) during $t = (0, 300)$ s, and then switched to $\delta_x = 1.7$ mm (= 10% of max shear) during $t = (300, 600)$ s. The δ_x is changed only in the x-direction so only the error in x is relevant. The absolute creep cannot be calculated over the whole measurement time-range as there were jumps in shearing distance δ_x which cause total decorrelation. Instead, the relative error between consecutive images, is calculated. Φ-images are recorded approximately every 10 seconds and Δ-images are calculated as a sequential subtraction

$$\Delta(T_n) = \Phi(T_n) - \Phi(T_{n-1}) \tag{14}$$

The relative error $E_{Rx}(T_n)$ is calculated as the difference between the creep-induced value on the left-most edge $x = x_L$ and right-most edge $x = x_R$ of the image:

$$E_{Rx}(T_n) = \frac{m_x\left[x_L,\, \Delta(T_n)\right] - m_x\left[x_R\, \Delta(T_n)\right]}{T_n - T_{n-1}} \tag{15}$$

for each Δ-image and represent the relative induced parasitic signal per second of duration of measurement.

The time-evolution of the relative error is shown in figure 5. Just after changing the shearing angle α_x the relative error E_R is very high, and drops to $E_R = 0.01\,\pi/\text{s}$ after around 30 s. In a typical medium-time-span shearographic measurement,

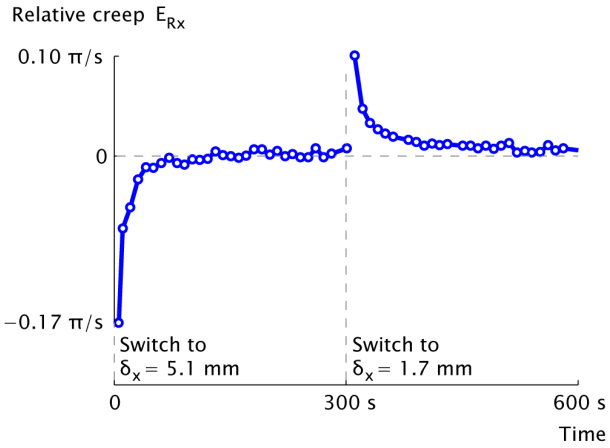

Figure 5: The relative creep E_{Rx} induced by the actuator controlling the shearing distance in the x-direction, δ_x. At $t = 0$ the shearing distance is set from $\delta_x = 0$ mm to $\delta_x = 5.1$ mm, and then switched to $\delta_x = 1.7$ mm at $t = 300$ s.

lasting 10 s, the relative error $E_R = 0.01\,\pi$/s would cause a 0.1π gradient over the image, a considerable error source. For the measurement setup used and a typical shearing distance of $\delta_x = 5$ mm, this is analogous to measuring a parasitic gradient of 3.3 µm/m.

After the parasitic signal, caused by the PZT creep of the shearing mirror, is removed by means of the equation 13, the noise in the images can be evaluated. In the next section the noise is quantified and related to the duration of the measurement. It is shown how much of an influence the environmental vibrations have.

4 Noise in the measurements and the effect of external vibrations

After the effect of the PZT creep is removed from the images, the noise increase with time is another problem of long time-span measurements. In this section the noise increase is quantified, in order to characterise the external vibrations and the general stability of the measurement system.

A single Δ-image can be represented by its histogram. A histogram shows the relative frequency at which a certain value occurs in an interval of values – bins – in an image. As the imaging CCD sensor is 8-bit, a single pixel can assume one of the $2^8 = 256$ values. The number of pixels that fall into each of the 256 bins is counted from a Δ-image and a histogram is constructed. A perfect Δ-image, with no deformation imposed, should be a zero-value image, and the histogram should show a distribution of noise around zero. The histogram for the Δ-image of the plate with no deformation, from figure 6a, is shown in figure 6b. A normal Gaussian distribution, characterized by its mean μ and standard deviation σ, appears to be a bad approximation for the distribution in the Δ-image, as can be seen in 6b. Estimating the noise in the shearography measurements using the concept of the

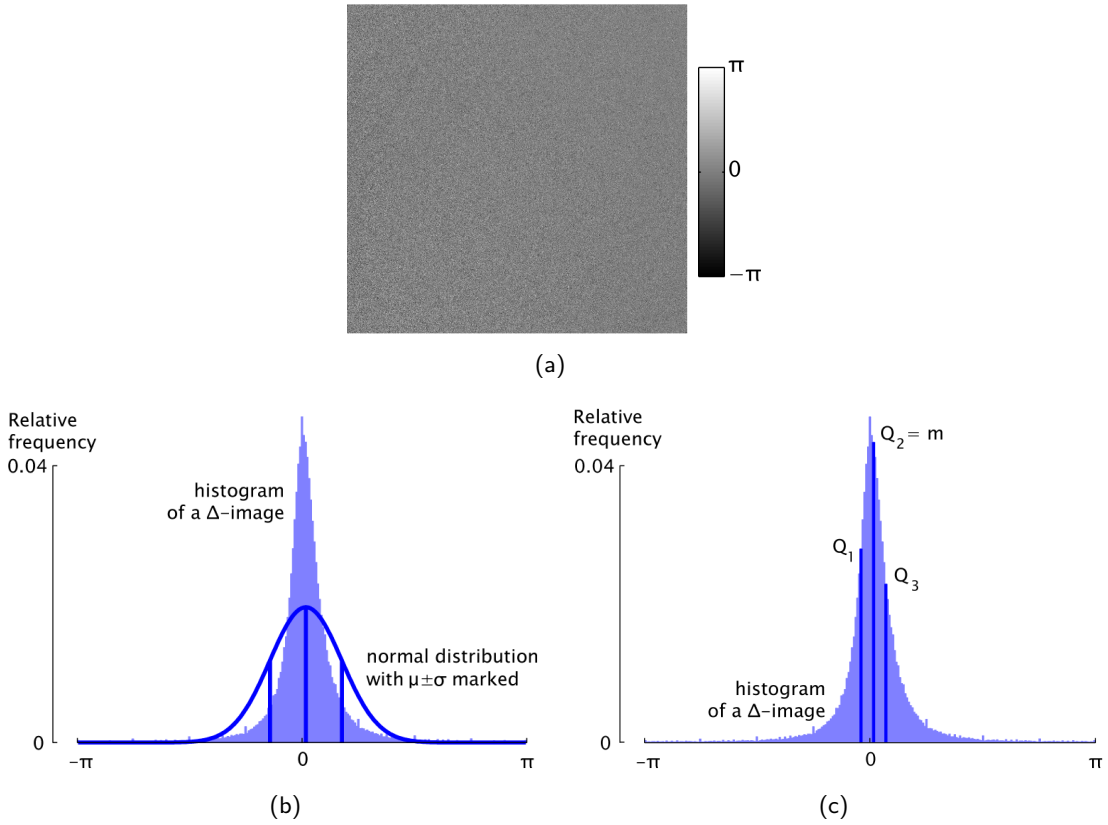

Figure 6: The distribution of the probability in a Δ-image (a) can be shown with a histogram (b and c). The normal distribution (b), which is defined by a mean μ and a standard deviation σ, provides a poor fit. Therefore, the more general distribution parameters, the lower quartile Q_1, the median $Q_2 = m$ and the upper quartile Q_3 are used (c).

mean μ and the standard deviation σ would thus be misguiding, as they are commonly linked to a Gaussian distribution of uncertainty, which shearography does not follow. Therefore, a more general approach using the quartiles for the statistical description of the noise will be used in this paper.

The distribution is represented by the quartiles – the lower quartile Q_1, the median Q_2 and the upper quartile Q_3. Quartiles divide the sorted group of pixel values from a Δ-image into 4 groups, each group containing a quarter of the pixel values. The lower quartile Q_1 is the value that separates the lowest 25% of the pixel values from the rest, median Q_2 splits the sorted pixel values into two equal-sized groups, and the upper quartile Q_3 separates the highest 25% of the pixel values. An interquartile range $IQR = Q_3 - Q_1$ is the width of the range that encompasses 50% of the values between the upper and the lower quartile. The figure 6c shows how the quartiles and the IQR describe the distribution.

The IQR would be zero for a zero-noise measurement, and all the pixels in the image would have a zero value. If the time between acquiring the Φ-images is allowed to increase, because of the external vibrations and the air currents,

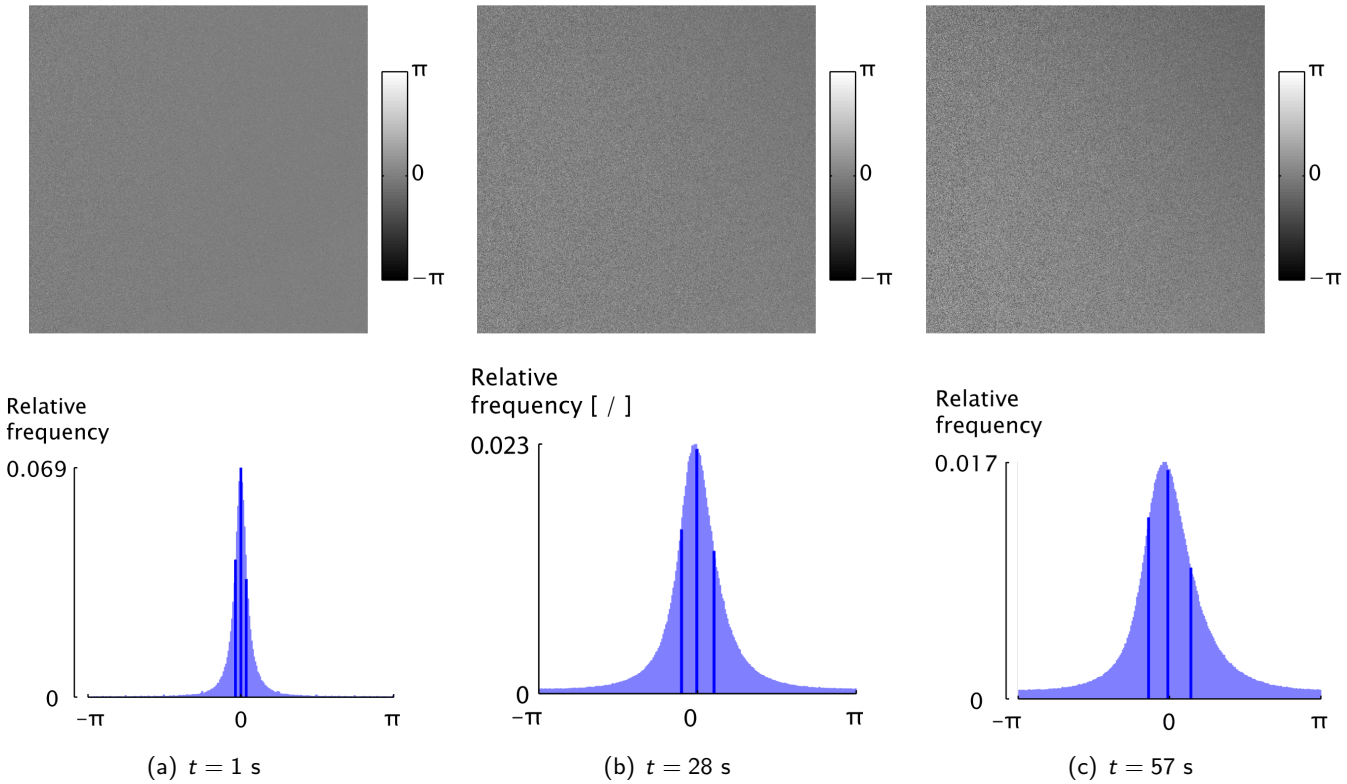

(a) $t = 1$ s (b) $t = 28$ s (c) $t = 57$ s

Figure 7: The Δ-images and their respective histograms for cases with different time t between acquiring the consecutive Φ-images. As the time t increases, so does the noise, making the histogram have a less pronounced peak.

the resulting Δ-image will have more noise. With more noise, the scatter of the values increases, thus increasing the IQR. As the IQR is increased, the peak at zero is less pronounced. This is demonstrated experimentally, for measurements with increasing time between acquisition of the two Φ-images, in the figure 7. Filtering of the images, a standard technique in shearography, makes the peak more pronounced and reduces the IQR, but all the conclusions in this paper are done for unfiltered images.

The noise evolution over time can be used to characterise the overall stability of the setup. The stability will be tested in 2 scenarios:

- the shearography setup and the test plate are mounted on a pneumatically-actuated vibration-isolating table,
- the shearography setup and the test plate are on the table with the pneumatic actuation turned off (so external vibrations are not damped)

The measurements are made by taking consecutive Φ-images, recorded approximately every 1 s. 1 s is the speed at which the camera can capture two consecutive Φ-images. As in the previous section, the measurements were done of a flat aluminium plate, with no deformation imposed. The Δ-images at time

$t = T_n$ are created by subtracting a Φ-image at time $t = T_n$ by the first Φ-image in the series, at $t = 0$ s. In shearography, this calculation of the Δ-image is called a static subtraction.

$$\Delta(T_n) = \Phi(T_n) - \Phi(0) \tag{16}$$

Compare the equation 16 with the previous equation 14, where the Δ-images are computed by sequential subtraction. Since the error is now computed from $t = 0$ to the $t = T_n$, it is the absolute error

$$\begin{aligned} E_A = &\Big| m_x\left[x_L, \Delta(T_n)\right] - m_x\left[x_L, \Delta(T_n)\right] \Big| + \\ &\Big| m_y\left[y_T, \Delta(T_n)\right] - m_y\left[y_B, \Delta(T_n)\right] \Big| \end{aligned} \tag{17}$$

where x_L and x_R are the coordinates of the left and right edge of the image, while y_T and y_B are the top and bottom.

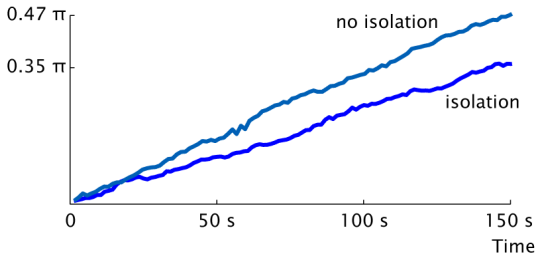

(a) E_A of the PZT creep removed from the images

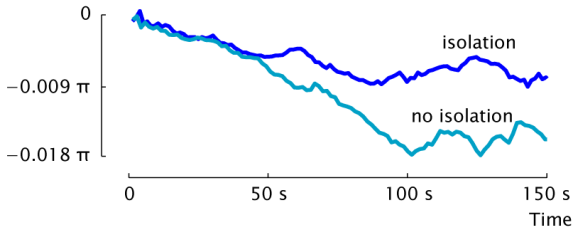

(b) median Q_2 after PZT creep is removed

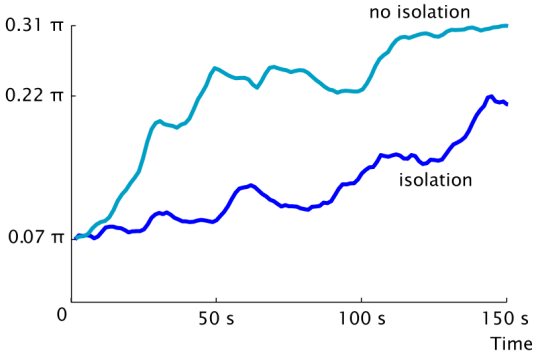

(c) IQR after PZT creep is removed

Figure 8: To show the effect of the environmental vibration isolation, experiments are performed in a time-span of 150 s. The parasitic signal related to the PZT creep (a) is first removed from the Δ-images, and the remaining parasitic signal is minor (b). With isolation, the noise in the measurements (characterized by the IQR) is considerably diminished (c).

The shearing is set in x-direction only (horizontal direction in the images), at the value corresponding to $\delta_x = 4.5$ mm for the setup involved.

The error due to the creep of the shearing PZT actuator is removed. The amount of error that is removed is visualized in figure 8a for both cases with and without the vibration isolation. The maximal systematic error shows a steady drift, linear with respect to time. In figure 8b the median of the pixel value distribution is calculated. It can be seen that even after the correction for the PZT creep, the median of the pixel values is still not exactly zero. The IQR shown in figure 8c is the representation of the noise evolution with time.

There are considerable differences between the two measurement scenarios, the non-isolated and the isolated. The active vibration-isolation reduces the noise very much. The noise level (IQR value) of the non-isolated table at $t = 50$ s is already equal to the noise level of the isolated setup after $t = 150$ s.

The experiments show clearly that the noise in the measurements is increasing with time. Because the creep of the PZT actuators is removed, the noise is related to the environmental vibrations, and the overall stability of the setup. The experiment used to quantify these values is very simple, and it can be used prior to any quantitative measurement. In the next section, some practical advices for users of shearography systems are given.

5 Practical approach for minimizing the noise in shearography

The previous section shows that minimizing the time for measurement of Δ-images in shearography is critical for acquiring high-quality images. The noise in the measurements is rising quickly, and in the case of medium (≈ 30 s), or long duration (> 60 s) measurements, a vibration-isolation is necessary for quantitative evaluation of the results.

The creep of piezo-electric actuators controlling the shearing distance can create a significant measurement error. For a long duration of the experiment of 150 s, it is shown that it can be up to 35% of the measurement range. The creep of the piezo-resistive actuators can be controlled by a closed-loop system, such as strain-gauge control, or directly, by dedicating a portion of the measurement field for the creep measurement. The creep of the shearing PZT actuator creates a linearly varying error field over the image. A portion of the image can be left undeformed and dedicated to calculating the effect of the PZT creep. Effect of the PZT shear creep is additive, so it can be easily removed, provided that the shear creep is known.

The simple noise and stability measurement, proposed in this paper, can be automated, and should be applied before conducting any quantitative shearography measurement. Results from the noise and stability measurements can be summarized by three coefficients, and used to characterise a shearography measurement setup. The first important value is the minimal IQR for a given measurement. The *minimal IQR* summarises the baseline uncertainty that can be expected in a given measurement, and depends on the shearography equipment settings, such as the opening of the aperture (controlling the speckle size), the exposure time for a single image, the amount of shearing in x and y, among others. It can be

Table 1: The uncertainty estimates (in an interval $(0, 30)$ s) for the two example measurements shown in figure 8

	minimal IQR	average spread of IQR	error from PZT creep
no isolation	$0.0707\,\pi$	$0.0044\,\pi/\mathrm{s}$	$0.0958\,\pi$
with isolation	$0.0694\,\pi$	$0.0010\,\pi/\mathrm{s}$	$0.0705\,\pi$

visualized as the minimal value in the figure 8c.

The second value describing the shearography setup is the *spread of the IQR*, meaning the average increase of the IQR with time for a given setup. In the figure 8c it can be visualized as the slope of the linear fit of the IQR with regard to time. The linear fit should be calculated for the expected duration of the measurements.

The third and final value relevant to describe the stability of the setup is related to the creep of the piezo-electric actuators controlling the shearing angles. For $t = 0$, the effect of the creep will be zero, and the factor of creep over time is the relevant value – the slope of the curve from the figure 8a.

The 3 characteristic values for the two measurements scenarios presented in this paper are given in table 1. The 2 measurement setups show the same minimal IQR as they were performed with same setting. The stability of the two setups is different, so the IQR spread is different for the two isolation cases. Error from the shear-actuator creep is similar for the no-isolation and the isolation case, as they were performed one after another.

Another advantage of doing these noise and stability measurements is the ability to estimate the measurement uncertainty. Given an expected measurement time T, the width of the range within which 50% of values fall is given by

$$\mathrm{IQR}(T_n) = \mathrm{IQR}_{min} + \mathrm{IQR}_{\mathrm{spread}}\, T_n \tag{18}$$

6 Conclusions

The paper has shown that PZT creep of the shearing actuator has a major impact on the quantitative measurements in shearography. It creates a parasitic signal that needs to be minimized or corrected. The PZT creep is in nature time-dependent and as such has a higher importance for long-term shearography measurements, like thermal loading cases or complex static deformation cases.

It is shown that the PZT creep creates an additive signal, which can be removed, if the amount of PZT creep is known. It is thus possible to reserve a part of the shearography image area specifically for measuring the PZT creep. For short-term measurements of a few seconds or fractions of a second, the PZT creep can be neglected.

Shearography is often claimed to be able to operate in industry conditions, and its relative insensitivity to environmental disturbance is praised. The investigation of time-dependent noise shows that, however, isolating the environmental vibrations has very beneficial influence on stability of the measurements. For

quantitative measurements, especially for longer time-span measurements, it is thus the opinion of the authors that environmental isolation is crucial.

In the last section of the paper some practical suggestions are given on how to quantify the influence of the PZT creep and how to estimate the time-dependent noise due to the environmental influences.

Acknowledgements

Part of this research has been sponsored by FWO, the Fund for scientific research of Flanders, Belgium.

References

[1] W. Steinchen and L. Yang, *Digital shearography: theory and application of digital speckle pattern shearing interferometry*. SPIE Press, 2003.

[2] D. Francis, R. P. Tatam, and R. M. Groves, "Shearography technology and applications: a review," *Measurement Science and Technology*, vol. 21, Oct. 2010.

[3] Y. Hung, "Digital shearography versus TV-holography for non-destructive evaluation," *Optics and Lasers in Engineering*, vol. 26, pp. 421–436, Mar. 1997.

[4] J. A. Leendertz and J. N. Butters, "An image-shearing speckle-pattern interferometer for measuring bending moments," *Journal of Physics E: Scientific Instrumentations*, vol. 6, pp. 1107–1110, 1973.

[5] Y. Y. Hung, "Shearography: A New Optical Method For Strain Measurement And Nondestructive Testing," *Optical Engineering*, vol. 21, no. 3, 1982.

[6] Y. Hung, Y. Chen, S. Ng, L. Liu, Y. Huang, B. Luk, R. Ip, C. Wu, and P. Chung, "Review and comparison of shearography and active thermography for nondestructive evaluation," *Materials Science and Engineering: R: Reports*, vol. 64, pp. 73–112, May 2009.

[7] Y. Hung, "Applications of digital shearography for testing of composite structures," *Composites Part B: Engineering*, vol. 30, pp. 765–773, Oct. 1999.

[8] P. Mäckel, H. Heyen, and W. Steinchen, "Die Scherografie: Ein quantitatives Messverfahren zur Schwingungs- messung und zerstörungsfreien Prüfung," *Laser Technik Journal*, vol. 1, no. 2, pp. 49–54, 2007.

[9] Y. Hung, W. Luo, L. Lin, and H. Shang, "Evaluating the soundness of bonding using shearography," *Composite Structures*, vol. 50, pp. 353–362, Dec. 2000.

[10] W. L. Lai, S. C. Kou, C. S. Poon, W. F. Tsang, S. P. Ng, and Y. Y. Hung, "Characterization of Flaws Embedded in Externally Bonded CFRP on Concrete Beams by Infrared Thermography and Shearography," *Journal of Nondestructive Evaluation*, vol. 28, pp. 27–35, Mar. 2009.

[11] Y. Hung and H. Ho, "Shearography: An optical measurement technique and applications," *Materials Science and Engineering: R: Reports*, vol. 49, pp. 61–87, Apr. 2005.

[12] G. De Angelis, M. Meo, D. Almond, S. Pickering, and S. Angioni, "A new technique to detect defect size and depth in composite structures using digital shearography and unconstrained optimization," *NDT & E International*, vol. 45, pp. 91–96, Jan. 2012.

[13] R. M. Groves, E. Chehura, W. Li, S. E. Staines, S. W. James, and R. P. Tatam, "Surface strain measurement: a comparison of speckle shearing interferometry and optical fibre Bragg gratings with resistance foil strain gauges," *Measurement Science and Technology*, vol. 18, pp. 1175–1184, May 2007.

[14] R. M. Groves, S. W. James, and R. P. Tatam, "Shape and slope measurement by source displacement in shearography," *Optics and Lasers in Engineering*, vol. 41, no. 4, pp. 621–634, 2004.

[15] F. Zastavnik, L. Pyl, J. Gu, H. Sol, M. Kersemans, and W. Van Paepegem, "Comparison of Shearography to Scanning Laser Vibrometry as Methods for Local Stiffness Identification of Beams," *Strain*, vol. 50, no. 1, pp. 82–94, 2014.

[16] D. C. Ghiglia and M. D. Pritt, *Two-Dimensional Phase Unwrapping: Theory, Algorithms, and Software*. Wiley-Interscience, 1998.

[17] H. A. Aebischer and S. P. Waldner, "A simple and effective method for filtering speckle-interferometric phase fringe patterns," *Optics Communications*, vol. 162, pp. 205–210, Apr. 1999.

[18] M. Lehmann, *Statistical theory of two-wave speckle interferometry and its application to the optimization of deformation measurements*. PhD thesis, Ecole Polytechnique Federale de Lausanne, 1998.

[19] D. T. Goto and R. M. Groves, "A combined experiment with simulation approach to calibrated 3D strain measurement using shearography," in *Proceedings of SPIE*, vol. 7387, pp. 73871J–73871J–10, 2010.

[20] J.-R. Lee, D.-J. Yoon, J.-S. Kim, and A. Vautrin, "Investigation of shear distance in Michelson interferometer-based shearography for mechanical characterization," *Measurement Science and Technology*, vol. 19, p. 115303, Nov. 2008.

[21] F. L. D. Scalea, J. B. Spicer, and R. E. Green, "Electronic Shearography with Thermal Loading for Detecting Debonds in Thick Polyurethane/Steel Panels

for Marine Applications," *Research in Nondestructive Evaluation*, vol. 12, no. 1, pp. 43–51, 2000.

[22] P. Hariharan, B. Oreb, and T. Eiju, "Digital phase-shifting interferometry: a simple error compensating phase calculation algorithm," *Applied optics*, vol. 26, no. 13, pp. 2504–2506, 1987.

[23] C. Joenathan, "Phase-measuring interferometry: new methods and error analysis," *Applied optics*, vol. 33, no. 19, pp. 4147–4155, 1994.

[24] S. Wu, L. Zhu, Q. Feng, and L. Yang, "Digital shearography with in situ phase shift calibration," *Optics and Lasers in Engineering*, vol. 50, pp. 1260–1266, Sept. 2012.

[25] D. Zhou and M. Kamlah, "Room-temperature creep of soft PZT under static electrical and compressive stress loading," *Acta Materialia*, vol. 54, pp. 1389–1396, Mar. 2006.